Characterization of a tunable, single-beam ponderomotive-optical trap

J. L. Chaloupka

Laboratory for Laser Energetics and Department of Physics and Astronomy, University of Rochester, 250 East River Road, Rochester, New York 14623-1299

D. D. Meyerhofer

Laboratory for Laser Energetics, Department of Physics and Astronomy, and Department of Mechanical Engineering, University of Rochester, 250 East River Road, Rochester, New York 14623-1299

Received June 17, 1999; revised manuscript received December 1, 1999

The generation and numerical and optical characterization of a single-beam, ponderomotive-optical trap are discussed. A novel segmented wave-plate technique is described, and experimental results of the trap formation are presented. Several methods to tune the traps are discussed, including techniques to realize a bright trap for dark-seeking electrons. The effects of non-Gaussian incident beams and beams with phase aberrations on trap formation are also described. © 2000 Optical Society of America [S0740-3224(00)02904-0]

OCIS codes: 000.2190, 020.7010, 140.3370, 140.7010, 350.5340.

1. INTRODUCTION

The motion of a charged particle interacting with an oscillating electromagnetic field can be decomposed into a high-frequency quiver motion and a slower, cycle-averaged drift. Although the Lorentz force is responsible for both components of the particle's motion, the slower motion is governed by the ponderomotive force. In the appropriate limits of a slowly varying field envelope (spatially and temporally), this force is proportional to the gradient of the field intensity, always pushing the charged particle away from regions of high field.[1–3] Because most field distributions (a Gaussian laser focus, for example) are centrally peaked, the consequence of this force is a repulsion of particles from the peak field region. By turning the direction of decreasing intensity inward, one can confine charged particles with a high-frequency electromagnetic field.[4] Specific laser-based schemes have been proposed to trap electrons in two dimensions,[5–7] and a three-dimensional electron trap was recently reported.[8] To our knowledge, this is the only trapping beam geometry to have been generated with a high-peak-power laser. It should be noted that this technique also works as an atom trap. As long as the laser is blue detuned to the atomic transition, the dipole force will push atoms away from bright regions. Blue-detuned dark traps, including a multibeam gravito-optic trap,[9] a scanning beam trap,[10] a doughnut-mode trap,[11] and single-beam, gravito-optic traps,[12,13] have been demonstrated. The trap described in this paper is novel in that it provides three-dimensional confinement that is due to the dipole force alone, without the need for crossing or scanning beams. This technique works with both continuous wave and pulsed lasers. Recently a similar scheme was used to trap atoms in the dark region of a single beam focus.[14]

The outline of this paper is as follows: Methods of altering a centrally peaked laser focus are discussed in Section 2. The novel segmented wave-plate scheme that is used to generate the trapping region is described in Section 3, and focal region scans experimentally obtained are presented in Section 4. The tunability of the trap and specific tuning schemes are presented in Section 5, and the effects of nonideal beams are discussed in Section 6. Some methods to verify electron trapping experimentally are described in Section 7, where the conclusion is presented. Recent observations of electron trapping with a high-intensity laser pulse are presented elsewhere.[15]

2. ALTERING THE LASER FOCUS

The three-dimensional focal region generated by passage of a spatially Gaussian, uniphase beam through a perfect lens is well known and calculable within the paraxial approximation.[16] Altering the incident beam or the focusing lens, however, makes an analytic calculation of the focus difficult. For this reason, a computer program has been written to calculate focal regions generated from arbitrary input conditions. The code is based on Huygen's principle, which states that one can consider every point on a wave front to be a point source for a spherical wave.[17] As a result, if the amplitude and the phase of a field are known in a source plane, one may add all the contributions from the individual spherical waves to determine the field at an observation plane. The code uses the Fresnel and the scalar-wave approximations. One can calculate the intensity profile in a three-dimensional region by scanning the observation plane along the laser propagation direction. The flexibility of this approach permits the use of any incident beam profile. A non-Gaussian intensity distribution may be used, phase terms

0740-3224/2000/050713-10$15.00

may be added to an otherwise uniphase beam, or a perfect lens may be tilted or given aberrations. The goal of this manipulation is to produce a trapping beam: namely, a focal region whose intensity gradients point outward in one or more dimensions (i.e., a focal region with a local intensity minimum).

The results of the numerical simulations (Figs. 1–5) are shown in the following representation. An image of the beam before focusing (near field) is shown in gray scale, where the darkest shades represent the regions of highest field (this standard is followed throughout the paper). Two cross sections of the far-field focal region are also shown. The first is the yz slice at $x = 0$ (where x and y are radial directions and z is the laser propagation direction) centered about the best focus ($x = y = z = 0$). The final image is at the focal plane (xy slice at $z = 0$). Figure 1 shows the numerical simulation of the focusing of a uniphase Gaussian beam. Figure 1(a) shows an image of the beam before focusing (near field), where w is its $1/e^2$ (in intensity) radius. The xz slice is shown in Fig. 1(b), where z_0 is the Rayleigh range and w_0 is the $1/e^2$ (in intensity) radius of the beam at best focus ($z = 0$). Figure 1(c) shows the focal spot at best focus. Inasmuch as this focal volume has no local minimum, it has no trapping regions whatsoever.

In practice, the easiest method of beam modification is to block portions of the beam in the near field, which results in energy losses with only slight changes to the shape of the focal region. The effect of blocking the center of the beam with a centered disk ($d_{\text{block}} = 2w$) is shown in Fig. 2. Figure 2(a) shows the near-field image of the incident beam. The yz slice of the focal region is shown in Fig. 2(b), and the beam at the focal plane is shown in Fig. 2(c). The effect of near-field blocking on the focal region is minimal (except for the energy loss), and the focal spot is centrally peaked. Because the amplitude mask is circularly symmetric about the center of the beam, all rz slices are identical to the one shown. The focus will be centrally peaked for all amplitude masks with a uniphase beam.

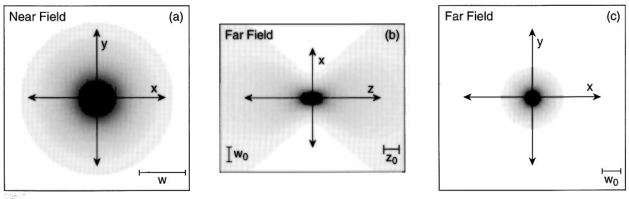

Fig. 1. A focused Gaussian beam forms a well-behaved, centrally peaked focal region. The first gray-scale image (a) shows the near-field intensity distribution. The second image (b) shows the intensity distribution as a function of z and x ($y = 0$); the center of the image corresponds to the best focus: $z = 0$, $r = 0$). The third image (c) shows the focal plane image at $z = 0$. The radii (at the $1/e^2$ point in intensity) of the incident beam (w) and the focal spot (w_0) are shown, along with the Rayleigh range (z_0). In these and all subsequent images, the darkest shades represent the regions of highest fields.

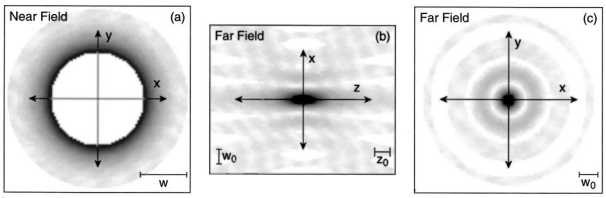

Fig. 2. Amplitude masking of the center of a Gaussian beam results in only small amplitude modulations in the focal region. The images are presented as in Fig. 1: (a) the near field, (b) the xz slice of the focal region, and (c) the focal plane image. The scaling shown is for the unaltered beam (Fig. 1).

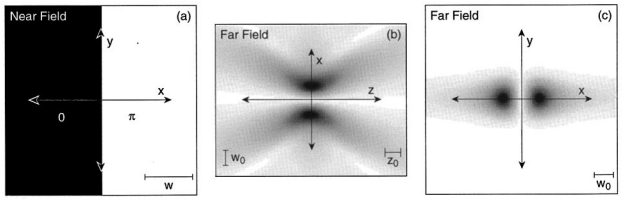

Fig. 3. Masking a Gaussian beam in the near field with a simple binary phase plate results in a drastic change in the focal region. (a) The two-level phase plate used to alter the focal region. (b) The xz slice of the altered focal region (the yz slice is devoid of a field). (c) The focal-plane image. The scaling shown is for the unaltered beam (Fig. 1).

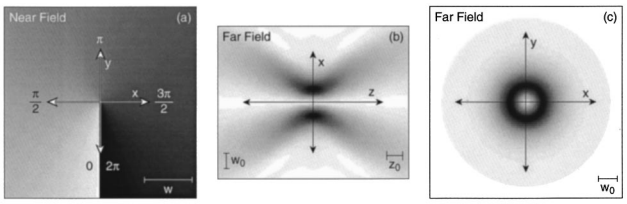

Fig. 4. A Gaussian beam focused after passing through a helical phase plate forms a highly altered focal region. (a) The smoothly varying helical phase plate. (b) The xz slice of the focal region. (c) The focal-plane image similar in shape to the doughnut mode (TEM_{01}^{*}). The scaling shown is for the unaltered beam (Fig. 1).

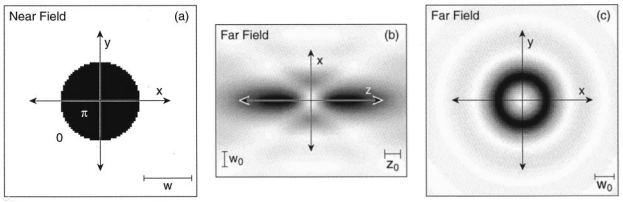

Fig. 5. A simple two-level phase plate alters the focal region primarily near best focus, creating a doughnut-shaped focal spot. (a) The two-level binary phase plate used to alter the focal region. (b) The xz slice of the focal region. (Because of the azimuthal symmetry of both the incident beam and the phase plate, the focal region is also azimuthally symmetric.) (c) The focal-plane image. The scaling shown is for the unaltered beam (Fig. 1).

Modifying the phase, rather than the amplitude, of the beam in the near field can result in deep far-field amplitude modulation with little loss in total energy,[18] which one can accomplish by placing phase masks in the path of the beam. Of particular interest has been the effect of binary phase plates, which add either a zero- or a π-phase shift to specific portions of the beam. If half of the incident Huygens wavelets are shifted by π and half are not, there will be complete destructive interference where they meet. For a focused laser beam, this destruction occurs at the center of the focal region ($r = 0$ and $z = 0$), which has been known for some time. Phase plates with

complex geometries have been manufactured to create small, on-axis null regions to aid in beam alignment.[19,20] A simple, two-zoned binary phase plate is shown in Fig. 3(a). It shifts the left half of the incident field by π with respect to the right half. The *yz* slice of the focal region is shown in Fig. 3(b) [z_0 and w_0 refer to the characteristics of the unaltered beam (see Fig. 1)]. Because the phase plate is not symmetric about the center of the beam, each *rz* slice is different. In the *yz* slice ($x = 0$), complete destructive interference occurs only along the laser axis. In the *xz* slice ($y = 0$), because the symmetry of the phase plate the beam destructively interferes completely throughout the entire slice. This becomes clear when one looks at the shape of the beam in the focal plane [Fig. 3(c)]. Such a focal region traps along only one dimension. One can generate a beam similar to the TEM_{01}^{*} mode (commonly referred to as the doughnut mode) by passing a Gaussian TEM_{00} beam through a smoothly varying helical phase plate [Fig. 4(a)]. Such phase plates have been generated for millimeter[21] as well as optical[22,23] wavelengths. The resultant focal region [Fig. 4(b)] is symmetric about the laser axis and therefore provides trapping along all radial directions but not along the laser propagation direction. The beam at the focal plane is shown in Fig. 4(c).

A much simpler binary mask [Fig. 5(a)] is composed of only two parts: a central disk of π phase and an outer, unshifted annulus. It produces a similar focal region near best focus to the doughnut beam but forms an intensity end cap on each side of the focus along the *z* direction [Fig. 5(b)]. This focal region is also symmetric for rotation about the laser axis. The beam at the focal plane is shown in Fig. 5(c). To satisfy the half-field-shifted criterion to create a null, the diameter of the π region (d_π) must equal 1.65 w, where w is the $1/e^2$ (in intensity) radius of the incident Gaussian beam. Expanded views of the trapping region are shown in Fig. 6(a) as a surface plot and Fig. 6(b) as a contour plot. The axes are labeled in normalized units (where I_0, w_0, and z_0 are the unaltered beam's peak intensity, beam waist, and Rayleigh range, respectively). The exact null at the center of the focus is surrounded on all sides by intensity walls that range from ~8% to ~30% of I_0. The region of complete, three-dimensional trapping has a volume of $\sim 2w_0^2 z_0$. A three-dimensional contour surface of the trapping volume is shown in Fig. 6(c).

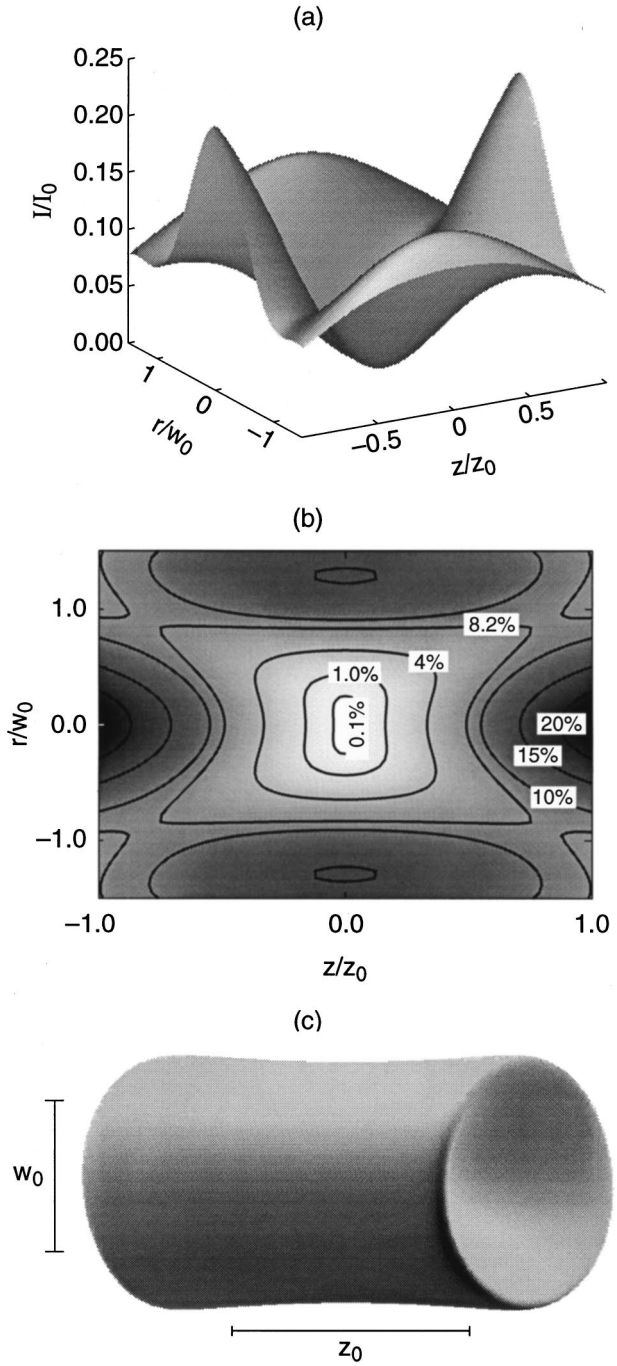

Fig. 6. Expanded view of the focal region generated by passage of a Gaussian beam (with $1/e^2$ in intensity radius equal to w) through a π-phase plate [with the diameter of the π region (d_π) equal to 1.65 w] as in Fig. 6. (a) Surface plot of the *xz* slice of the focal region. Because of the azimuthal symmetry, all *rz* slices are identical. (b) Contour plot of the trapping region. The contour lines represent the percent values of the peak intensity of the unaltered beam (i.e., in the absence of the phase mask). (c) Contour surface of the three-dimensional trapping region, corresponding to the 8.2% contour line.

3. SEGMENTED WAVE-PLATE SCHEME

In general, phase masks can be generated by photolithographic techniques; however, for the particularly simple geometry (the central π region) that produces the trapping region a novel segmented wave-plate approach has been developed.[8] A half-wave plate is typically used to rotate the polarization direction of an incident, linearly polarized beam of light. The birefringent nature of the wave-plate material (e.g., mica) causes light polarized along one of its optical axes to travel at a different speed from light polarized along the other axis. The slower-moving beam is polarized along the ordinary axis (*o* wave), whereas the faster-moving beam is polarized along the extraordinary axis (*e* wave). A π-phase shift between the two polarizations results from a careful choice of thickness for a given incident wavelength. If part of a beam can be made to travel as an *o* wave while the rest travels as an *e* wave, a π-phase shift between the two portions will result. Cutting a circular section from the cen-

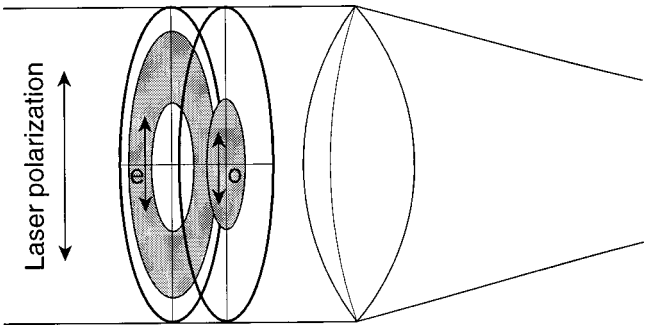

Fig. 7. Experimental setup for the segmented wave-plate technique for generating a trapped focal region. The annulus has an 80-mm outer diameter and a 41-mm inner diameter; the disk has a 39-mm diameter.

ter of a half-wave plate and reinstalling it with a 90° rotation can achieve the exact effect of the two-level π plate. In Fig. 7, which shows this arrangement, the laser polarization is vertical, coinciding with the e axis of the outer annulus and the o axis of the inner disk. If half of the incident field passes through the disk and the other half passes through the annulus, the half-field-shifted criterion to create a null is met. The scheme works equally well for an incident beam with an arbitrary, but uniform, polarization. In general, the electric field of the incident beam (as a plane wave) can be described as

$$\mathbf{E}(z, t) = \hat{i}E_{0x}\cos(kz - \omega t) + \hat{j}E_{0y}\cos(kz - \omega t + \epsilon), \tag{1}$$

where $\hat{i}$ and $\hat{j}$ are unit vectors perpendicular to the direction of laser propagation. When the y axis is lined up with the o axis of the inner disk and the e axis of the outer annulus, the resultant field is expressed as

$$\mathbf{E}_{\text{inner}}(z, t) = \hat{i}E_{0x}\cos(kz - \omega t + \phi) + \hat{j}E_{0y}\cos(kz - \omega t + \epsilon + \phi + m\pi) \tag{2a}$$

$$= \hat{i}E_{0x}\cos(kz - \omega t + \phi) - \hat{j}E_{0y}\cos(kz - \omega t + \epsilon + \phi), \tag{2b}$$

$$\mathbf{E}_{\text{outer}}(z, t) = \hat{i}E_{0x}\cos(kz - \omega t + \phi + m\pi) + \hat{j}E_{0y}\cos(kz - \omega t + \epsilon + \phi) \tag{3a}$$

$$= -\hat{i}E_{0x}\cos(kz - \omega t + \phi) + \hat{j}E_{0y}\cos(kz - \omega t + \epsilon + \phi), \tag{3b}$$

where m is an odd integer ($m = 1$ for a zero-order half-wave plate) and ϕ and ($\phi + m\pi$) are the optical path lengths through the wave plate for light polarized along the e and the o axes, respectively. So, for an arbitrary polarization, $\mathbf{E}_{\text{inner}}(z, t) = -\mathbf{E}_{\text{outer}}(z, t)$. If half of the incident field passes through each region, the field at the center of the focus will be made up of equal parts of $\mathbf{E}_{\text{inner}}$ and $\mathbf{E}_{\text{outer}}$ and will therefore completely destructively interfere. This is true for all values of m for a plane wave. For a short pulse, the extra path between the e and o axes must be small compared with the temporal length of the pulse, $m\pi \ll \omega\tau$, where τ is the laser pulse width. The total number of cycles in a pulse is $N_{\text{cycles}} = \omega\tau/2\pi$, so the condition on the order of the wave plate can be written as $m \ll 2N_{\text{cycles}}$. For a 2-ps, 1-μm pulse, $2N_{\text{cycles}} \sim 1000$, so this condition is easily met with any commercially available, multiorder half-wave plate.

4. EXPERIMENTAL RESULTS

To create a trapping focal region in the laboratory we machined a pair of wave-plate pieces for use with a Nd:glass, tabletop terawatt (T^3) laser system.[24] A 4-cm disk was cut from the center of an 8-cm mica half-wave plate by a 1-mm-thick cookie-cutter tool. Because of the large beam size (~7 cm), the small ring of material lost in the machining process was unimportant. For smaller beams, a separate disk and annulus could be machined from a single, oversized piece of mica.

To image the focal region, we aligned the wave-plate arrangement and a plano–convex focusing lens ($f = 212$ cm, $\phi = 15$ cm) to the path of the T^3 beam and placed a CCD camera coupled to a 10× microscope objective at the focus. The CCD camera array measured 4.8 mm by 3.6 mm (512 × 492 pixels) and was captured by an image card through a personal computer as a digital image (256 × 242 pixels). The microscope objective was mounted approximately 7 cm from the CCD array (measured from the shoulder of the objective to the array) to give a magnification of ~5×. By moving the camera–objective combination along the laser propagation direction, we made scans of the focal region. To map out the focal region in detail, we made a scan with a continuous-wave beam (the upcollimated oscillator of the T^3 laser). Figure 8(a) shows the beam profile in the focal plane and the $1/e^2$ (in intensity) radius of the unaltered beam. Figure 8(b) shows the slice in the xz plane, and Fig. 8(c) shows the slice in the yz plane. The region of complete trapping is shown in each plot and is bound by the solid contour line of 10% of the unaltered beam's peak intensity. The intensity at the center of the trapping region is less than 2% of the unaltered beam's peak intensity. Slices along other planes have similar profiles. This explicitly demonstrates the generation of a large ($V \sim w_0^2 z_0/2$) and fairly deep region of three-dimensional, ponderomotive-optical trapping.

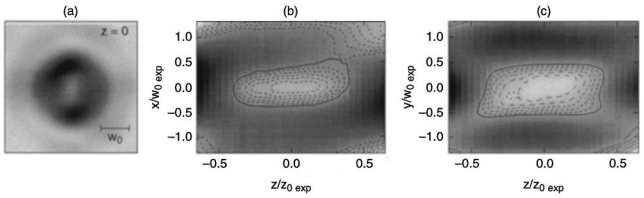

Fig. 8. Focal-plane image and contour plots of the trapping focal region generated with a continuous-wave beam (the upcollimated output of a Nd:YLF oscillator) and the segmented wave plate. (a) The beam at best focus ($z = 0$). The beam radius for the unaltered beam ($w_{0\,\text{exp}}$) is shown. (b) Image of the xz slice of the focal region (taken by scanning the camera through the focal region) with the corresponding contour plot. Dashed curves indicate intensity values of 7.5%, 8.0%, 8.5%, 9.0%, and 9.5% of the unaltered beam's peak intensity. The solid curve corresponds to 10.0% of the unaltered beam's peak intensity and surrounds the region of complete, three-dimensional trapping. (c) The yz slice.

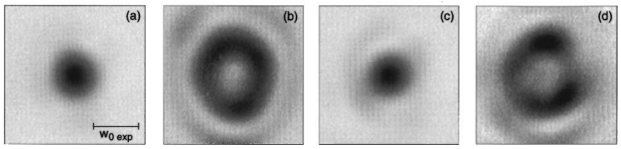

Fig. 9. Focal-plane images at $z = 0$ taken with a single laser pulse ($E \sim 40$ mJ, $\tau \sim 2$ ps, $\lambda \sim 1$ μm): (a) without the wave-plate arrangement in place, (b) with the wave-plate setup in place and set to 90°, (c) with the wave-plate setup in place and set to 0°, (d) with the wave-plate setup at 90° and $E \sim 500$ mJ.

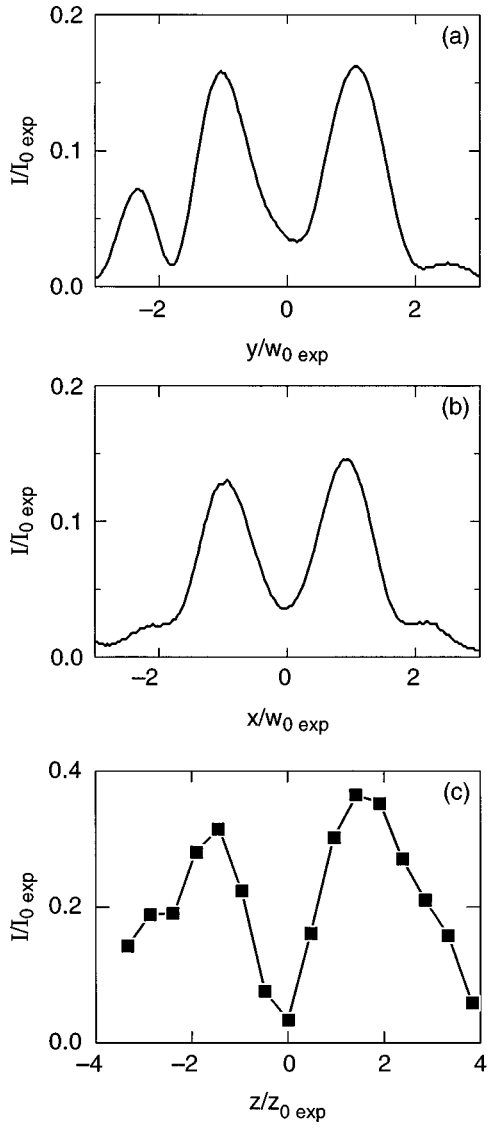

Fig. 10. Lineouts of the trapping focal region taken with a moderate-power, pulsed laser beam [as in Fig. 10(b)]. (a) Lineout in the x direction (at best focus: $z = 0$). (b) Lineout in the y direction ($z = 0$). (c) The intensity at $r = 0$ as a function of z (the discrete points represent the camera position through the z scan). All axes are normalized to the experimentally determined values for the unaltered beam (spot size for the x and y positions, Rayleigh range for the z positions, and unaltered beam peak intensity for the intensity values).

A scan with moderate- and high-power pulsed beams (~40 or ~500 mJ, ~2 ps, ~1 μm) was also made. Figure 9(a) shows the focal-plane image created at moderate power without the wave-plate arrangement in place. Figure 9(b) shows the focal-plane image with the wave-plate arrangement in place and set at 90° (i.e., the o axis of the inner disk coincides with the e axis of the outer annulus and vice versa). Figure 9(c) shows the focal-plane image with the wave-plate arrangement set to 0°, and Fig. 9(d) shows the focal-plane image with the wave-plate arrangement in place and set to 90° and the laser firing at high power. Figure 10 shows intensity lineouts of the trapping volume [corresponding to Fig. 9(b)] along three directions. The lineout at $x = 0$ and $z = 0$ (along the y direction) is shown in Fig. 10(a), and the lineout at $y = 0$ and $z = 0$ (along the x direction) is shown in Fig. 10(b). Figure 10(c) shows the lineout at $x = 0$ and $y = 0$ (along the z direction). The discrete points in this plot represent the single-shot intensity along the laser axis (at $r = 0$) at each camera position. The axes are labeled in terms of the experimentally obtained characteristics of the unaltered beam, where $w_{0\,exp}$ is the radius at best focus, $z_{0\,exp}$ is the Rayleigh range, and $I_{0\,exp}$ is the peak intensity. As expected, the minimum at the center of the focal region is bounded in three dimensions by regions of higher intensity. It is clear that the segmented wave-plate scheme is compatible with a high-peak-power laser system and that it produces trapping regions in agreement with predictions.

5. TUNING THE TRAP

For some applications, a trapping beam with an exact null at the center of the focal region is desirable; however, to force the trapped particles to interact with a strong field it is advantageous to create a region with a local, but nonzero, minimum. For example, electrons interacting with an intense oscillating electromagnetic field quiver aharmonically because of the nonlinearity of the Lorentz force. As a result, harmonics of the incident field are emitted.[2,25,26] The strength of this emission depends linearly on the interaction time of the electrons and nonlinearly on the field strength. Harmonics of the incident field were recently observed from a nontrapping focus.[26] To enhance this effect, a trapping focus with a high field at its center is ideal. In atom trapping, such a trap can be made with an ordinary, centrally peaked beam that is red detuned to the atomic transition. This is clearly a bright trap, as the atoms are attracted to the intense focus.[27] A blue-detuned beam repels atoms and must therefore have a local minimum in order to trap. This is a dark trap,[9–14] as the atoms spend most of their time in the dark region between the trap walls. Because electrons always seek low fields (regardless of the frequency of the electromagnetic field), a focus must have a local minimum to confine electrons. In this paper, a dark trap will have the ordinary meaning (i.e., a null in intensity surrounded by walls of nonzero intensity), whereas a bright trap will be defined as a focal region with a nonzero local minimum. This is the only bright trap possible for dark-seeking electrons.

The two-level, circular π plate and the segmented wave-plate arrangement are both tunable, resulting in focal regions with adjustable field strengths at their centers. The most obvious method for generating bright traps is not to comply exactly with the half-field-shifted

criterion described above. Altering the phase plate or the incident beam size such that either more or less than half of the incident field is shifted, will ensure that the destructive interference at the center of the focus will not be complete. For an appropriate choice of the size of the π region, a trapping focus (i.e., a focal region with a local minimum) is generated that has a significant percentage of the unaltered beam's peak intensity (I_0) at its center. This incomplete destructive interference will occur at the center of the focus for both undersized and oversized π regions. An undersized π region, however, results in a focal spot with a local maximum rather than a nonzero local minimum at its center. Figure 11 shows the focal-plane image profiles for several values of the diameter of the π region (d_π). For some values of d_π smaller than 1.65 w, a trapping region is formed with a bright center, but the minimum intensity within the trap is located away from the center and is equal to zero. Electrons confined in such a region will drift toward the zero-field regions. For a range of values of d_π larger than 1.65 w, a trapping region is formed with a bright minimum at its center. Such a trap confines electrons in a high-field region. This technique creates a bright trap for dark-seeking electrons.

Figure 12 shows the trap brightness ($I_{\min}/I_0$) and the trapping volume as functions of (oversized) d_π. The brightness is plotted as the percentage of the unaltered beam's peak intensity, and the volume is normalized to a characteristic volume of the unaltered beam ($w_0^2 z_0$). The solid curve corresponds to the minimum intensity within the trapping region, and the dashed–dotted curve corresponds to the minimum height of the trap wall. The distance between these curves represents the trap depth. The short-dashed curve corresponds to the volume of the region of complete trapping. Increasing the size of d_π causes a dark trap to become increasingly bright at the expense of trap depth and volume.

Although this method for generating bright traps is effective, it requires the manufacture of multiple phase plates (or wave-plate pieces) or different beam sizes. To bypass this problem one may place the phase plate or the segmented wave plate (with $d_\pi = 1.65\ w$) after the focusing lens. When the z location of the phase plate is varied, the size of the inner disk with respect to the beam's local radius will change. Because the beam is full sized near the lens, placing the phase plate at this position will result in a dark trap (corresponding to the far-left portion of Fig. 12). As the phase plate is placed farther from the lens, the beam converges and the size of the inner disk becomes effectively larger. As long as the phase plate remains in the near field of the incident beam (within the realm of geometric optics), the trap generated will be identical to that created with a collimated beam and a larger inner disk size but with the added spherical aberration that comes from passing a converging beam through a flat plate. The amount of aberration depends on the focusing strength and the thickness of the phase-plate substrate. (In Section 6 below we discuss the effects of spherical aberration on the trapping beam.) For a placement at 0.35 f from the lens (where f is the focal length of the focusing lens), the effective size of the inner disk will be equivalent to 2.55 w (the far right of Fig. 12). By scanning the phase plate one can realize the entire range of dark to bright traps.

The segmented wave-plate arrangement can also be used to tune the trap. When the inner and outer pieces are set to 90° with respect to each other and the diameter of the inner disk (d_{inner}) equals 1.65 w, the resultant focal region is a dark trap (identical to the one shown in Fig. 6) with a single polarization direction (y). If the outer annulus is rotated by θ_{outer}, the outer part of the beam will have its polarization rotated by $2\theta_{\text{outer}}$. At the focus, this polarization can be separated into terms along x and y and is equal to $\sin(2\theta_{\text{outer}})x + \cos(2\theta_{\text{outer}})y$. Light po-

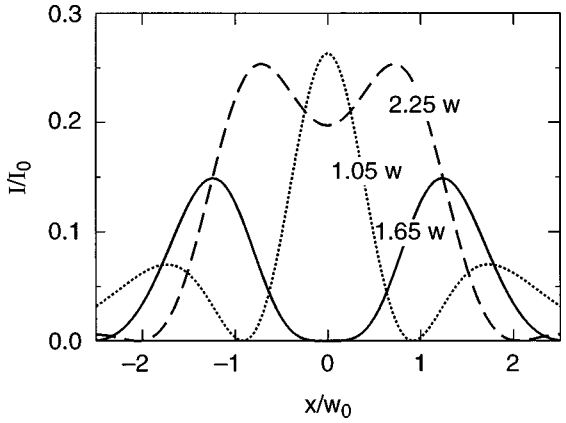

Fig. 11. The transverse lineouts of focal spots generated by three different phase plates show how the brightness at the center of the trap varies with the size of the inner π region. The solid curve shows an ideal dark trap generated with the half-field-shifted criterion ($d_\pi = 1.65\ w$). The dotted curve shows a dark trap with a bright center ($d_\pi = 1.05\ w$). Here, electrons will still be pushed into the region of the null field. The dashed curve shows an ideal bright trap ($d_\pi = 2.25\ w$). Here, trapped electrons are forced to interact with the central region of high field.

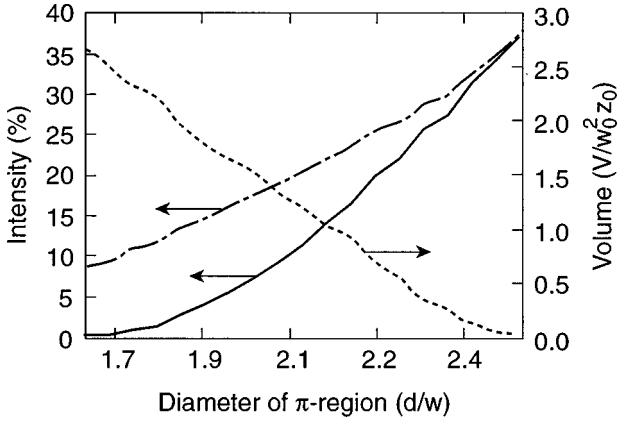

Fig. 12. Tuning the trap. The dashed–dotted curve represents the height of the trap wall (given in terms of the unaltered beam's peak intensity), and the solid curve represents the minimum intensity within the trap. The distance between these lines is the trap depth. The short-dashed curve represents the trap volume in terms of a characteristic volume for the unaltered focus $w_0^2 z_0$). The arrows indicate the vertical axis for each curve. One can best realize the transmission from a dark to a bright trap by altering the size of the inner π region. As the trap brightens, it becomes shallower and smaller. One can duplicate this effect by placing the phase plate or the wave-plate arrangement at an appropriate distance behind the focusing lens.

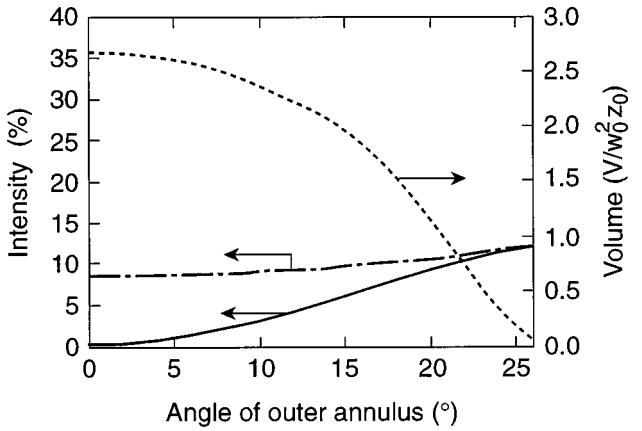

Fig. 13. One can generate a bright trap by rotating the outer annulus of the wave-plate arrangement ($d_{\text{inner}} = 1.65\ w$). Zero degrees corresponds to the ideal annulus orientation, where the *o* axis of the annulus lines up with the *e* axis of the disk and vice versa (performing in the same way as a π-phase plate). Ninety degrees corresponds to an ordinary half-wave plate. The curves in this plot are drawn as in Fig. 13.

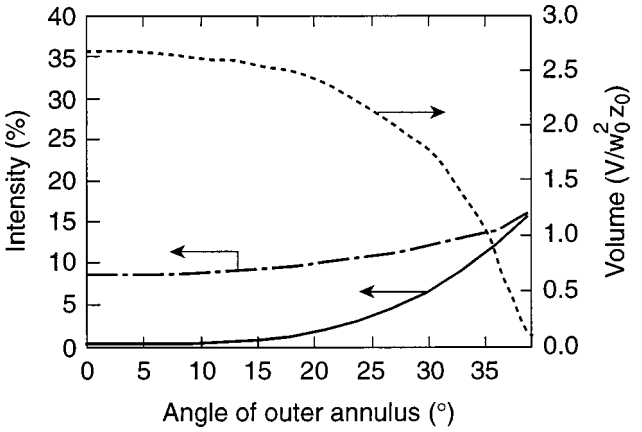

Fig. 14. Rotating the outer annulus (as in Fig. 14) and passing the beam through a polarizer can make the trap slightly brighter with the added benefit of only a single polarization in the beam. The curves in this plot are drawn as in Fig. 13.

larized along x will not interfere with light from the inner disk and will therefore add as an intensity. If $0° < \theta_{\text{outer}} < 45°$, light polarized along y will be π shifted and will interfere destructively with light from the inner portion of the beam. If $45° < \theta_{\text{outer}} < 90°$, light polarized along y will no longer be shifted and will add constructively. If $\theta_{\text{outer}} = 90°$, then the original, unaltered wave plate will be reconstructed. For some values of θ_{outer}, a bright trap will be generated. Figure 13 shows the trap brightness and volume as a function of θ_{outer}. Because the light rotated into the x polarization does not interfere with the y-polarized light, it adds as an intensity, and the central part of the trap fills in while the wall height remains nearly constant. This places a limit (approximately equal to the wall height for θ=0) on the brightness of the trap.

Removing the x-polarized light from the beam before the focusing lens generates larger and slightly brighter trapping regions. One can do this in practice by passing the beam through a polarizer after the wave plate that discards the light polarized along x. Figure 14 shows the trap characteristics as a function of θ_{outer} for this arrangement.

An effective solution for generating both bright and dark traps with a single arrangement (placed in a single position) is to use wave-plate pieces with an oversized d_{inner} and to pass the beam through a polarizer after the wave-plate pieces. Because of the presence of the polarizer, any rotation of either the disk or the annulus effectively attenuates that portion of the beam. Rotating the disk reduces the excess field in the inner portion of the beam to the proper half-field-shifted level for a dark trap. Rotating the annulus makes the inner portion effectively larger, and the trap center becomes even brighter. Figure 15 shows the trap characteristics as a function of the angles of the wave-plate pieces for $d_{\text{inner}} = 2.00\ w$. Although this scheme does not create a wide range of dark and bright traps as effectively as does varying d_π, it provides an alternative to making multiple phase plates when placing optics after the focusing lens proves difficult (e.g., the focusing lens is held within a vacuum chamber or in other tight quarters). It also eliminates the added spherical aberration that results from passing a converging beam through a flat plate.

6. EFFECTS OF ABERRATIONS AND NONIDEAL BEAMS ON TRAP FORMATION

The focal regions calculated up to this point have used a perfect, uniphase Gaussian beam incident upon an ideal lens. In this section the effects of nonideal focusing and non-Gaussian beams on the characteristics of the trap are described. To describe the beam after the lens, we combine a Gaussian amplitude distribution with the phase imparted by a perfect lens. An ordinary plano–convex lens gives a spherical phase distribution:

$$\Phi(r) = k(f^2 - r^2)^{1/2}, \tag{4}$$

where f is the focal length of the lens and $r^2 = x^2 + y^2$ is the square of the radial position along the lens. The code

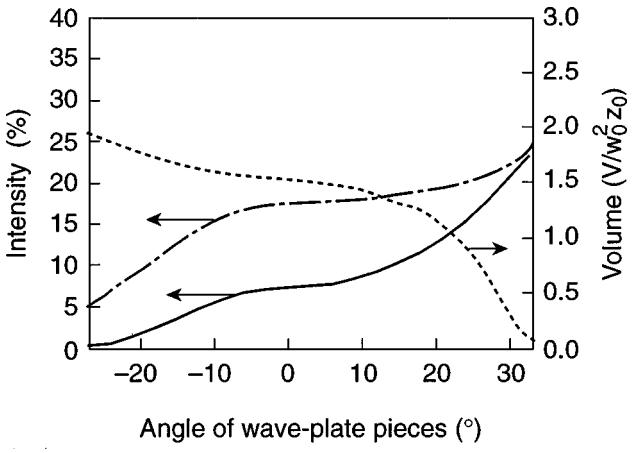

Fig. 15. By using a wave-plate arrangement with an oversized inner disk ($d_{\text{inner}} = 2.00\ w$) and passing the beam through a polarizer, one can tune the trap by rotating the inner disk to create a dark trap (corresponding to the negative angle values) or by rotating the outer annulus to create a bright trap (corresponding to the positive angle values). The curves in this plot are drawn as in Fig. 13.

adds the appropriate amount of phase to the beam but does not account for any bending of the light through the lens. This is a good approximation close to the axis of the lens, so with the paraxial approximation ($f^2 \gg r^2$) a binomial expansion gives

$$\Phi(r) = kf(1 - r^2/2f^2 - r^4/8f^4 - \dots). \tag{5}$$

The first term adds a constant phase to the entire beam and can be discarded, as can the higher-order terms because they are vanishingly small. The quadratic term gives the description of a perfect lens:

$$\Phi_p(r) = -kr^2/2f. \tag{6}$$

For a Gaussian incident beam, the calculated focal region is identical to the well-known analytical solution of a Gaussian laser focus. In practice, ideal lenses are not purely parabolic.

In modeling the effect of spherical aberration, the highest-order terms are included in the description of the focusing lens. The phase distribution for a lens with spherical aberrations is given as

$$\Phi_s(r) = \Phi_p(r) + A[\Phi(r) - \Phi_p(r)], \tag{7}$$

where A reflects the amount of aberration added. The lens is free of aberrations for $A = 0$ and is equivalent to a plano–convex lens (with the no-bending approximation) for $A = 1$. The dominant aberration term is proportional to r^4/f^3, so the amount of added phase for a given value of A depends strongly on the incident beam size and the focal length of the lens. The number of waves of spherical aberration (N_{sa}) at the $1/e^2$ (in intensity) radius *(w)* of the incident beam is a good measure of the strength of the aberration. Figure 16 shows the trap brightness (solid and dotted–dashed curves) and volume (short-dashed curve) as a function of N_{sa}. The thicker curves are normalized to the peak intensity of the aberration-free beam, and the thinner curves are normalized to the peak intensity of the nontrapping beam with spherical aberration. For $N_{sa} < 1/2$, the trap forms nicely and is larger, brighter, and shallower than in the aberration-free case. For larger values of N_{sa}, the trap volume falls off rapidly. In practical terms, it is advisable to use an aspheric focusing lens if an ordinary lens results in a large N_{sa} ($N_{sa} < 0.05$ for a dark trap; $N_{sa} < 0.5$ for a bright trap). For a purely spherical lens (e.g., plano–convex or biconvex), the value of N_{sa} is approximately equal to $w^4/8f^3\lambda$ (the leading aberration term with radius r set to incident beam waist w). The value of N_{sa} for the focusing lens and beam size used for Figs. 8–10 (from Section 4) was approximately 0.01.

Astigmatism is the presence of two different effective focal lengths along two different axes. If the axes are orthogonal, the astigmatism is considered to be regular and can be generated by tilting of the focusing lens. We did this mathematically in the computer code to study the effect of astigmatism on the trapping volume. If the lens is tilted about the x axis by an angle ϕ_{lens}, the effective focal lengths along the x and the y directions (for small ϕ_{lens}) are, respectively,[28]

$$f_x = f, \tag{8}$$

$$f_y = f \cos^2 \phi_{lens}. \tag{9}$$

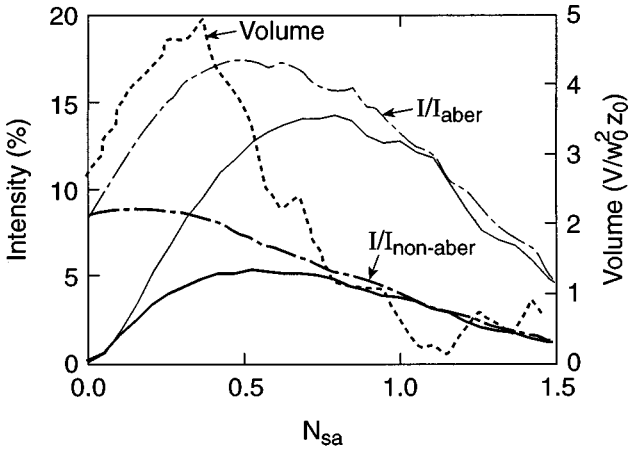

Fig. 16. Effects of spherical aberrations on the trap brightness, depth, and volume shown as a function of the number of waves of spherical aberration (N_{sa}) at the $1/e^2$ (in intensity) radius *(w)* of the incident beam. The thicker solid and dashed curves represent the minimum trap intensity and the height of the trap wall, respectively, normalized to the peak intensity of the nontrapping, nonaberrated beam. The thinner curves are normalized to the peak intensity of the nontrapping, aberrated beam. The short-dashed curve represents the trap volume normalized to the characteristic volume ($w_0^2 z_0$) of the nontrapping, nonaberrated beam. The short-dashed curve corresponds to the right vertical axis (volume), and all other curves correspond to the left vertical axis (intensity).

Despite this apparent separation into x and y components, the focal region along the yz plane is not merely a duplicate of the xz plane shifted by Δf. The field at every point within the focus is determined by integration along both dimensions of the incident beam. If we assume a simple focal shift in one dimension with respect to the other, however, the trapping region in the xz plane must overlap in the z direction with the trapping region in the yz plane. Effectively, this means that the distance between trap centers must be smaller than the trap length. The distance between trap centers is $\Delta f = f_x - f_y$, and the trap lengths are approximately equal to $1.5\, z_0$; so, for overlapping to occur, $\Delta f/z_0$ must be less than 1.5. The amount of lens tilt that this corresponds to depends on the incident beam size and the focal length of the lens. For a given ϕ_{lens}, Δf is proportional to f and z_0 is proportional to f^2/w^2, so $\Delta F/z_0$ is proportional to w^2/f. Figure 17 shows the trap brightness (thick and thin solid and dashed–dotted curves) and volume (short-dashed curves) as a function of $\Delta f/z_0$. As the astigmatism worsens, the trap shrinks and becomes brighter and shallower. A focal scan of the nontrapping beam is sensitive enough to permit us to predict whether the astigmatism in a system will be too severe to generate a trapping beam. A Gaussian beam with an astigmatism corresponding to $\Delta f/z_0 = 1.5$ has an aspect ratio (equal to r_x/r_y, where r_x and r_y are the $1/e^2$ radii in the x and the y directions, respectively) of 1.8 at $z = 0$ (where $z = 0$ is a distance f_x from the lens).

As was shown in Section 2, beams with non-Gaussian amplitude profiles generally produce centrally peaked focal regions; however, the effect on the trapping region depends on the particular shape of the near field. An extreme example of a non-Gaussian shape is a doughnut

beam created by blocking of the central portion of a Gaussian beam. Figure 18(a) shows the near field of the incident beam. The block has an outer diameter of 2 w, and d_π is set to 2.6 w. After the incident beam has passed through an appropriately sized phase plate, the shape of its shifted and unshifted regions are quite similar (both are doughnuts), so the focal regions generated by the sections are similar. As a result, the destructive interference at the center of the focus is strong. Figure 18(b) shows a surface plot of an rz slice of the focus. The regions near $z = 0$ are dim even away from $r = 0$, so the trap is shallow in the radial direction. The enclosed trapping volume has an outer intensity value of only 3.0% of the nontrapping beam's peak intensity (generated with the doughnut-shaped incident beam), with a null at the center. We can make another nonideal beam profile by blocking an annular section of a Gaussian beam. Figure 18(c) shows the near field of the incident beam. The block has an inner diameter of 1.0 w and an outer diameter of 2.5 w. This choice results in a perfect null at the center of the focus when the inner portion of the beam is shifted with respect to the outer section. In this case the two sections are quite dissimilar, and therefore their focal regions are alike only near the center of the focus. Fields away from this point do not interfere destructively and consequently form higher trap walls. Figure 18(d) shows a surface plot of an rz slice of the focal region. The enclosed trapping volume has an outer intensity value of 18.4% of the nontrapping beam's peak intensity (generated with the annulus-blocked incident beam), with a null at the center. In both cases the intensity values are normalized to the peak intensity of the blocked beams focused without the phase plate. In the second case, if the values are instead normalized to the peak intensity of the ordinary, unblocked beam, then the outer intensity value will drop to 3.3%. Clearly there is no advantage in blocking a properly shaped Gaussian beam when one is generating a trapping focus.

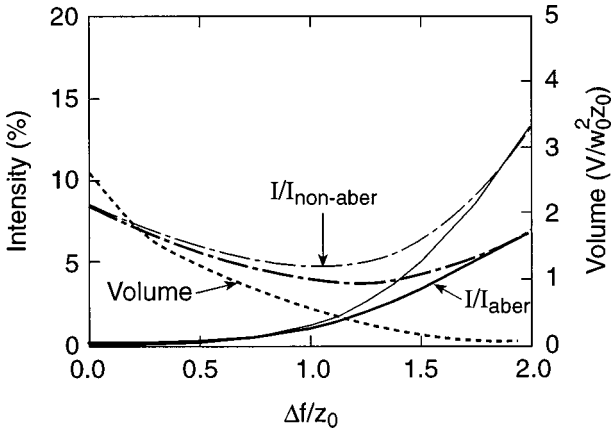

Fig. 17. Effects of astigmatism on the trap brightness, depth, and volume shown as a function of the astigmatic focal-length difference (Δf) divided by the Rayleigh range of the nonaberrated beam (z_0). The curves in the plot are drawn as in Fig. 17.

7. CONCLUSION

A trapping focal volume with an intensity minimum at the center has been created by use of a segmented wave plate. We have extended this study numerically to examine different trapping configurations and the effect of aberrations. It is possible to trap energetic electrons with a high-peak-power laser beam by use of this method.[15] A novel scheme to create a trapping focal region has been presented, along with focal images of the trapping beam generated with a T^3 laser. Methods of tuning the center trap intensity have been discussed, and the destructive effects of nonideal incident beams have been analyzed and shown to be controllable. The effect of laser aberrations is small enough that the trap will be created even with imperfect beams. The enhanced interaction of the electrons with the laser beam will result in several detectable signatures of trapping. The trapped electrons themselves will leave the laser focus after a much longer and more complicated interaction with the field and will exhibit highly unusual trajectories. Electrons ejected from a Gaussian laser focus are ejected primarily perpendicularly to the laser axis.[29] Trapped electrons will be ejected across a wide spread of angles—from far forward to far backward. In addition, the high-density confinement of electrons in the trapping region will increase the likelihood of their recombination with ions, thereby increasing the emission of recombination light from the center of the focus. Inasmuch as there is an increased interaction of electrons with the field even for a dark trap, the electrons will scatter the incident radiation for a longer period of time and will therefore enhance Thomson scattering.[15] Finally, the strong electron–laser interaction within a bright, high-intensity

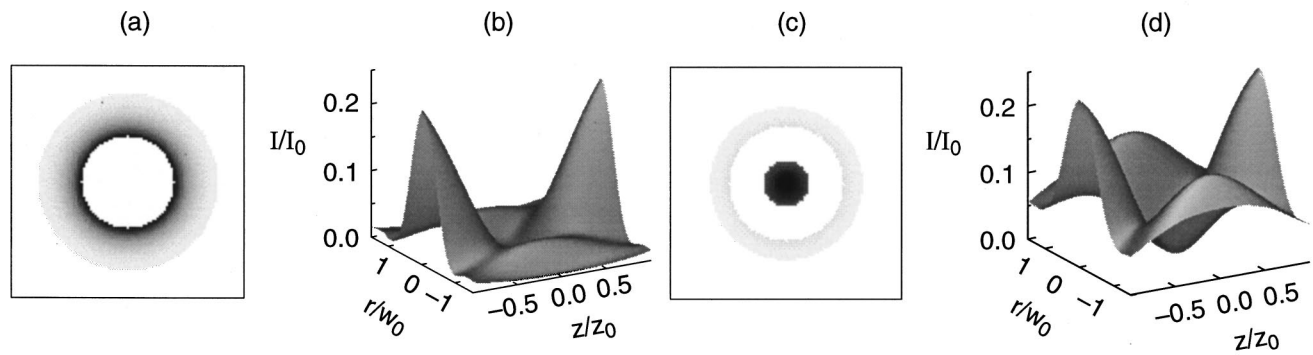

Fig. 18. Dark trapping focal regions generated by non-Gaussian beams: (a) a centrally blocked Gaussian in the near field and (b) a surface plot of the trapping region; (c) a Gaussian near field with an annular block and (d) a surface plot of the trapping region.

trap will increase the emission of harmonic radiation from oscillating free electrons, thereby enhancing the recently observed nonlinear Thomson scattering of light from relativistic electrons.[26]

ACKNOWLEDGMENTS

The authors thank A. Maltsev for machining the λ/2 plate. We also thank N. P. Bigelow, J. H. Eberly, Y. Fisher, and T. J. Kessler for helpful discussions. This research was supported by the National Science Foundation, with additional support from the U.S. Department of Energy (DOE) Office of Inertial Confinement Fusion under cooperative agreement DF-FC03-92SF19460, the University of Rochester, and the New York State Energy Research and Development Authority. The support of the DOE does not constitute an endorsement by the DOE of the views expressed in this paper.

REFERENCES

1. H. A. H. Boot and R. B. R.-S. Harvie, "Charged particles in a non-uniform radio-frequency field," Nature **180**, 1187 (1957).
2. E. S. Sarachik and G. T. Schappert, "Classical theory of the scattering of intense laser radiation by free electrons," Phys. Rev. D **1**, 2738–2753 (1970).
3. J. H. Eberly, "Interaction of very intense light with free electrons," in *Progress in Optics*, E. Wolf, ed. (North-Holland, Amsterdam, 1969), Vol. 7, pp. 359–415.
4. V. Gapanov and M. A. Miller, "Potential wells for charged particles in a high-frequency electromagnetic field," J. Exp. Theor. Phys. **34**, 242–243 (1958).
5. N. J. Phillips and J. J. Sanderson, "Trapping of electrons in a spatially inhomogeneous laser beam," Phys. Lett. **21**, 533–534 (1966).
6. U. Mohideen, H. W. K. Tom, R. R. Freeman, J. Bokor, and P. H. Bucksbaum, "Interaction of free electrons with an intense focused laser pulse in Gaussian and conical axicon geometries," J. Opt. Soc. Am. B **9**, 2190–2195 (1992).
7. C. I. Moore, "Confinement of electrons to the center of a laser focus via the ponderomotive potential," J. Mod. Opt. **39**, 2171–2178 (1992).
8. J. L. Chaloupka, Y. Fisher, T. J. Kessler, and D. D. Meyerhofer, "Single-beam, ponderomotive-optical trap for free electrons and neutral atoms," Opt. Lett. **22**, 1021–1023 (1997).
9. H. J. Lee, C. S. Adams, M. Kasevich, and S. Chu, "Raman cooling of atoms in an optical dipole trap," Phys. Rev. Lett. **76**, 2658–2661 (1996).
10. P. Rudy, R. Ejnisman, A. Rahman, S. Lee, and N. P. Bigelow, "All-optical dynamical dark trap for neutral atoms," submitted to Phys. Rev. Lett.
11. T. Kuga, Y. Torii, N. Shiokawa, T. Hirano, Y. Shimizu, and H. Sasada, "Novel optical trap of atoms with a doughnut beam," Phys. Rev. Lett. **78**, 4713–4716 (1997).
12. J. Yin and Y. Zhu, "Dark-hollow-beam gravito-optical atom trap above an apex of a hollow optical fibre," Opt. Commun. **152**, 421–428 (1998).
13. Yu. B. Ovchinnikov, I. Manek, A. I. Sidorov, G. Wasik, and R. Grimm, "Gravito-optical atom trap based on a conical hollow beam," Europhys. Lett. **43**, 510–515 (1998).
14. R. Ozeri, L. Khayovich, and N. Davidson, "Long spin relaxation times in a single-beam blue-detuned optical trap," Phys. Rev. A **59**, R1750–R1753 (1999).
15. J. L. Chaloupka and D. D. Meyerhofer, "Observation of electron trapping in an intense laser beam," Phys. Rev. Lett. **83**, 4538–4541 (1999).
16. P. W. Milonni and J. H. Eberly, "Laser resonators," in *Lasers* (Wiley, New York, 1975), pp. 484–490.
17. Ref. 16, pp. 511–514.
18. L. W. Casperson, "Spatial modulation of Gaussian laser beams," Opt. Quantum Electron. **10**, 483–493 (1978).
19. J. Ojeda-Castañeda and G. Ramírez, "Zone plates for zero axial irradiance," Opt. Lett. **18**, 87–89 (1993).
20. S. B. Viñas, Z. Jaroszewicz, A. Kolodziejczyk, and M. Sypek, "Zone plates with black focal spots," Appl. Opt. **31**, 192–198 (1992).
21. G. A. Turnbull, D. A. Robertson, G. M. Smith, L. Allen, and M. J. Padgett, "The generation of free-space Laguerre–Gaussian modes at millimetre-wave frequencies by use of a spiral phaseplate," Opt. Commun. **127**, 183–188 (1996).
22. M. W. Beijersbergen, R. P. C. Coerwinkel, M. Kristensen, and J. P. Woerdman, "Helical-wavefront laser beams produced with a spiral phaseplate," Opt. Commun. **112**, 321–327 (1994).
23. H. He, N. R. Heckenberg, and H. Rubinsztein-Dunlop, "Optical particle trapping with higher-order doughnut beams produced using high efficiency computer generated holograms," J. Mod. Opt. **42**, 217–223 (1995).
24. Y.-H. Chuang, D. D. Meyerhofer, S. Augst, H. Chen, J. Peatross, and S. Uchida, "Suppression of the pedestal in a chirped-pulse-amplification laser," J. Opt. Soc. Am. B **8**, 1226–1235 (1991).
25. Vachaspati, "Harmonics in the scattering of light by free electrons," Phys. Rev. **128**, 664–666 (1962).
26. S.-Y. Chen, A. Maksimchuk, and D. Umstadter, "Experimental observation of relativistic nonlinear Thomson scattering," Nature **396**, 653–655 (1998).
27. S. Chu, J. E. Bjorkholm, A. Ashkin, and A. Cable, "Experimental observation of optically trapped atoms," Phys. Rev. Lett. **57**, 314–317 (1986).
28. R. S. Longhurst, *Geometrical and Physical Optics* (Wiley, New York, 1967), pp. 365–366.
29. C. I. Moore, J. P. Knauer, and D. D. Meyerhofer, "Observation of the transition from Thomson to Compton scattering in multiphoton interactions with low-energy electrons," Phys. Rev. Lett. **74**, 2439–2442 (1995).